PEG-Mediated Silica Pore Formation Monitored in Situ by USAXS and SAXS: Systems with Properties Resembling Diatomaceous Silica

Qianyao Sun,* Theo P. M. Beelen, and Rutger A. van Santen

Eindhoven University of Technology, Schuit Institute of Catalysis, P.O. Box 513, 5600 MB Eindhoven, The Netherlands

Sandra Hazelaar, Engel G. Vrieling, and Winfried W. C. Gieskes

University of Groningen, Department of Marine Biology, P.O. Box 14, 9750 AA Haren, The Netherlands

Received: April 24, 2002; In Final Form: August 26, 2002

Poly(ethylene glycol) (PEG) was employed as templating agent for the synthesis of porous silica. The effect of PEG chain length and of the PEG/silica ratio on textural properties (fractality, pore size, and pore distribution) were investigated by monitoring the development of silica-PEG intermediates using ultrasmall and small-angle X-ray scattering analysis with high-brilliance synchrotron radiation to obtain sufficient radiation intensity for dynamic results at the subminute scale. We show that even a simple structure-directing polymer, such as PEG, results in silicas with pores of diameters spanning a range of less than 2 nm up to 20 nm, depending on polymer molecule length and polymer/silica ratio. Flocculation may well be the most important distinction between silicas prepared with small and large PEG. In this view, small PEG600 gets encapsulated by silica and forms pools within the silica framework, whereas large PEG20,000 is entangled in a mass of silica spheres, making enclosure by silica or phase separation impossible. Both polymer chain length and the polymer/silica ratio govern the relative importance of flocculation, phase separation, and hydrophobic silica-PEG interactions steering the silica polymerization. Increase in hydrophobicity results in a larger surface area and a more uniform pore size distribution, an effect confirmed by scanning electron microscopy (SEM) and observations of physical adsorption of nitrogen gas (BET). Polymers, such as PEG, may well be an inexpensive and versatile substitute and model for polypeptides known as structure-directing agents in biomineralization if silicas resembling natural ones, notably the ones present in such a huge diversity in algae of the group of diatoms, are the focus of scientific attention, e.g., for biomimicking with a view on industrial applications.

Introduction

Extensive work has been undertaken to prepare (meso)porous silicas and to understand the complicated physical chemistry accompanying the relatively simple condensation reaction where silica monomers are used to build the large polymeric structures typical for such porous silicas.[1−3] Although the most beautiful silica architecture is still built by nature (for example, the skeletons of diatoms[4]),[16] man-made silicas have made impressive progress. Especially the introduction in 1992 of the MCM-materials, using surfactants as structure-directing agents,[5] brought the development of methods to prepare mesoporous silicas forward with a great leap; the insight was born that a template was not just a molecule on its own (as in most of the zeolites), but that cooperative effects between molecules could produce very big templates. In the MCM-systems mentioned, surfactants as alkyltrimethylammoniumbromide (alkyl = C_{12}−C_{18}) form micelles, and during the polymerization of silica the space around and between the micelles is occupied with amorphous silica. After removal of the surfactant, regular mesopores are formed that are moreover much bigger than the pores in most zeolites.[3]

In addition to the increased size of the structure-directing agents, a second fundamental property appeared to be extremely important. The polymerizing silica also had a strong influence on the formation of the micelles, resulting in different micelles and different mesoporous silicas if the surfactant/silica ratio was changed. For example, Vartuli et al.[6] studied the effect of the surfactant/silica ratio, and Stucky et al.[7] constructed a synthesis phase diagram of a TEOS/CTAB/NaOH system (silica/water = 100), showing that besides the hexagonal phase (MCM-41) also a cubic phase (MCM-48) and a lamellar phase (MCM-50) could be prepared, all depending on gel composition.

Although increasing the chain length of the alkyl group or improving the synthesis conditions add many nanometers to the pore size or induce better stability or increase the pore size distribution, the large and no doubt controlled pore dimensions observed in diatoms[4,8] were still out of range using quaternary ammonium surfactants. But guided by these results, many other types of surfactants (cationic, anionic, and amphiphilic) and commercially available polymers have been applied as structure-directing agent, resulting in numerous new mesophases as reviewed by Saraya et al.[9]

From our investigations concerning biogenic silica formation in diatoms,[8,10,11] to eventually apply the knowledge gained therefrom to make better (industrial) mesoporous silicas, specific proteins have been identified to be present during the synthesis. The groups of Morse and Stucky isolated such proteins, e.g., silicatein in sponge biosilica.[12,13] They mimicked the properties of this protein by synthetic cysteine-lysine block copolypeptides,[14] which resulted in several silica morphologies. Kröger

* Author for correspondence. Email: q.sun@tue.nl.

10.1021/jp026011r CCC: $22.00
Published on Web 10/09/2002

et al.[15] isolated peptides (called silaffins) from diatom cell walls and obtained networks of silica nanospheres almost immediately after addition of silaffins to a solution of silicic acid. However, using diatomaceous proteins as templates to prepare porous silica is still only possible on a very limited scale: it is difficult to isolate these proteins in quantities required for more comprehensive research or bulk synthesis. Therefore, we have chosen for modeling Nature's use of proteins by using polymers as models. Because serine groups are important in silicatein[12] or silaffins,[15] and can be extracted from silica of diatoms,[10] we have chosen poly(ethylene glycol) (PEG), an inexpensive, nonionic, hydrophobic, and water-soluble polymer, as a model-template or structure-directing agent. The general formula is $HO(CH_2-CH_2-O)_nH$ and the numbers in PEG600, PEG2000 and PEG20000 refer to the average molecular weight, with $n \approx 12$, 45, and 455, respectively.

Because the formation of vesicles or micelles by PEG[17,18] strongly depends on cosolvents, silicic acid (from water glass) was chosen as the silica source instead of TEOS or similar silica compounds, avoiding the formation of ethanol during the hydrolysis. Moreover, to mimic the preparation of biogenic silica in diatoms, silicic acid is the most logic choice. Many papers have been published on the use of PEG (or PEG-based block-copolymers) as structure-directing agents during the preparation of silica (e.g., refs 19−32 and references therein), not only showing that the reaction is very complicated and that mesophases are formed during the silica polymerization but also that the phase separations are very sensitive for relatively small changes in reaction conditions, and that the rich structural and morphological transformations are due to the delicate hydrophilic/hydrophobic balance in the self-organization of the system.[29,33] Moreover, a complication that is not mentioned in most studies is the ability of PEG to operate as a flocculation agent, already mentioned by Iler.[1] Addition of a small amount of flocculant to a sol of silica particles leads to flocculation of only a portion of the colloidal particles, and if more is added, increasing amounts are precipitated. If sufficient flocculant is added to cover the surface of the particles, however, the sol is stabilized again with repulsive or nonattracting polymer-clad particles.[1,34,35] Applying light scattering, the flocculation of silica particles using PEG was studied by Wong et al.[36] Ågren et al.[19] discerned stable and phase-separated systems during the preparation of PEG-silica, depending on the molecular weight of the PEG polymers, and in this case phase separation was ascribed to flocculation.

When a PEG-silica composite is synthesized, organization on length scales from (sub)nanometer to microns is important. At short length scales, information on the ordering of molecules or oligomers (silicic acid and its primary particles) can be obtained. Subsequently, the growing silica-PEG intermediates are typically in the nanometer range, whereas the produced silicas can grow in the micrometer range. To probe the complete broad range of length scales involved in the assembly process, we used a combination of small- and ultrasmall angle scattering of X-rays (SAXS and USAXS, respectively). With the appropriate combination of stations and setups, we were able to probe length scales from 2 nm to about 6000 nm. Because of the high brilliance of the synchrotron radiation (resulting in short acquisition times) we could perform in situ experiments on PEG-silica preparations in dedicated cells.[39] To obtain reliable information concerning intermediates during the preparation, it is not possible to study dried or otherwise processed samples, because then the very vulnerable species will be changed immediately; only a noninvasive approach, such as the one used for our study, is the alternative. Once the reaction is completed, the synthesis mixture can be dried, washed, and calcined, allowing the investigation of the resulting porous silica with controlled adsorption of nitrogen gas (BET-method) and scanning electron microscopy (SEM).

In this paper we attempted to recognize the different roles of PEG as structure-directing agent, as flocculating agent, and in phase separation. Therefore we also analyzed the intermediates during the preparation of PEG-silicas in order to find relations between the applied species or quantity of PEG andthe pore structure of the calcined silicas.

Experimental Section

Sample Preparation. The sodium silicate solution (27 wt % SiO_2, 8 wt % Na_2O, analytical grade, Merck) was diluted 4-fold prior to preparation. Three varieties of poly(ethylene glycol) (PEG) were used: PEG600, PEG2000, and PEG20000, with molecular weights of 600, 2000, and 20 000, respectively (Merck). PEG-mediated silica was synthesized by dissolving 0.75 or 3.00 g of PEG (respectively for a $C-C-O/SiO_2$ ratio of 0.5 and 2.0) in water (30 mL solution) and mixing this with 45 mL of 1 M solution of hydrochloric acid. Under vigorous stirring, 30 mL of a 4-fold diluted silicate solution was added dropwise, followed by a few drops of a diluted NaOH (0.1 M) solution to reach the desired pH of 4.00 ± 0.03. In this way both the pH and the concentrations were kept constant in every experiment. Since 4-fold diluted sodium silica solution was added and vigorous stirring was employed, no significant change was observed in all synthesis systems. Silica precipitation in the samples occurred after about one-half hr for PEG2000 and 20 000, and several minutes later for PEG600.

Immediately after the preparation the stirrer was stopped and for USAXS and SAXS the dedicated cell was filled with approximately 1 mL of this reaction mixture (liquid or gel, depending on the presence and molecular weight of PEG). The solution or gel was allowed to gelate during 1 h at room temperature (RT), followed by two hrs aging at 80 °C. For nitrogen adsorption experiments (BET) and scanning electron microscopy (SEM) solid samples were obtained by drying (16 h at 80 or 90 °C) the wet gel, followed by washing to remove NaCl and calcination (4 h at 550 °C) to prepare PEG-free porous silica. These samples were prepared both at Grenoble and at the home laboratory of Eindhoven University, prior to the powder scattering experiments in Grenoble. No differences between the Grenoble- and Eindhoven-prepared samples could be observed. According to thermal gravimetrical analyses (TGA), the silicas appeared to be PEG-free after calcination.

SAXS and USAXS. Both SAXS and USAXS experiments were performed at the European Synchrotron Radiation Facility (ESRF, Grenoble, France). For SAXS the beamlines ID02 (wavelength $\lambda = 0.154$ nm; camera length = 2 m) and BM26 (DUBBLE) (wavelength $\lambda = 0.118$ nm; camera length = 10 m) were applied, providing the domains $0.1 < Q < 3.1$ nm^{-1} and $0.05 < Q < 1$ nm^{-1}, respectively, for the Q range ($Q = (4\pi/\lambda)\sin(\theta/2)$, with θ = scattering angle) and corresponding with length scales $2 < d < 60$ nm and $6 < d < 120$ nm, respectively. Because of the high-intensity synchrotron radiation and position-sensitive detectors, acquisition times between 1 s and 1 min were sufficient to provide SAXS patterns with optimal signal-to-noise ratios.

USAXS experiments were also performed at beamline ID02 using a Bonse-Hart camera ($0.001 < Q < 0.316$ nm^{-1} or $20 < d < 6000$ nm).[38] A configuration with two analyzer crystals was used, so no desmearing was necessary. The wavelength of

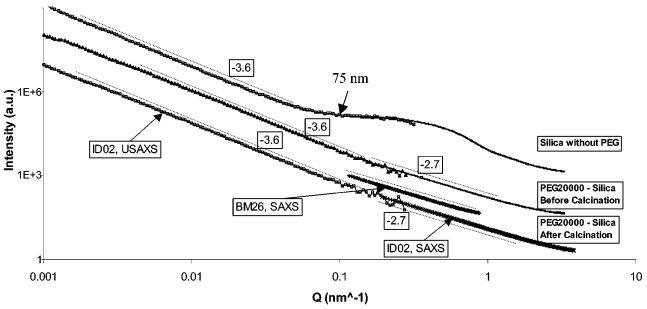

Figure 1. Merging of USAXS/SAXS patterns of (1) PEG20,000-Silica (after calcination, lower curve). At the left: USAXS at ID02. In the middle: SAXS at DUBBLE (BM26). At the right: SAXS at ID02, (2) PEG20,000-Silica (before calcination, middle curve), (3) silica made in the absence of PEG (after calcination, upper curve). The scattering profiles were plotted against scattering wave vector Q, where Q is related to the scattering angle (θ) and the wavelength of the incident X-ray (λ) by $Q = (4\pi/\lambda)\sin(\theta/2)$. Intensities have been shifted vertically at the log(I) scale during the merging process, but the slope (fractal dimension) has been preserved during the processing.

the X-rays was 0.1 nm. A NaI scintillator was used as the detector, which shows a linear response over 4 decades of intensity. Because of the high brilliance of the undulator beamline ID2, a complete USAXS pattern could be recorded in only 15 min, despite the inherent low efficiency of the Bonse−Hart setup and the scanning mode of recording.

The raw data was normalized for the intensity of the X-ray beam and corrected for detector sensitivity prior to background correction. The scattering from water at the reaction temperature and from adhesive tape were used as a background pattern for in situ reaction mixtures and solid samples respectively; background subtraction was applied according to the procedure introduced by Vonk.[37] For the calibration of the SAXS patterns, the scattering of wet rat-tail collagen was used. The optics of USAXS were calibrated using Stöber-type silicas.[38]

Although SAXS and USAXS data had to be obtained in separate experiments it is very informative to have an overview of the complete Q range. To be able to merge the patterns of the three Q ranges, it is not only necessary to carry out exactly the same in situ preparations of silica during the USAXS and SAXS experiments including a perfect reproducibility but also the presence of a substantial overlap of scattering of the borderlines of the Q ranges. Finally the $I-Q$ axes have to be rescaled and the intensity expressed in arbitrary units.[39,40]

In merging of USAXS and two SAXS profiles in Figure 1 (lower curve), the slopes of the three profiles at the overlap portion appear a bit different at the end of the curve. The reason is that the measurement is close to the monitoring limit of the equipment, therefore the strength of scattered electrons is quite low and not totally reliable. So the combination of USAXS and SAXS data for an accurate structure study is quite necessary. Figure 1 also shows the silica samples before (middle curve) and after calcination (lower curve). It is clear that after calcination the curve turns more linear probably because of the smoothing of the rough surface. Therefore the USAXS/SAXS data of solids presented in this work are all from the calcined samples. Figure 1 also shows the silica solid sample prepared in the absence of PEG (upper curve). Similar to PEG-silica, the slope is −3.6 in the low Q region (USAXS). However, a big hump was observed in high Q region (SAXS), probably composed of many short-ranged fractals at size smaller than 75 nm.

To perform in situ experiments both for SAXS and USAXS investigations, a dedicated cell was applied, consisting of an electrically heated brass holder with a rotating round sample cell.[39] A rotation speed of 2 rpm was provided to keep the synthesis mixture as homogeneous as possible. Because only a very small spot near the center of the cell was exposed to the X-ray beam, a circular path of the sample was scanned continuously. Two thin (about 10 μm) mica windows were used as windows, with spacing provided by a Teflon ring (thickness, 0.5 mm). The liquid was heated hydrothermally up to 80 °C. Heating of the sample holder from RT to the reaction temperature of 80 °C took only 2 min.

Because of the very strong scattering of the porous silicas and to avoid multiple scattering, solid samples had to be investigated by sticking a very small quantity of powder onto adhesive tape.

Scanning Electron Microscopy (SEM). A scanning electronic microscope (JSM-840A, JEOL) was employed for the observation of the morphology of dried gels. Powdered samples, sticking onto adhesive tape, were used to examine the morphological variation after sputter coating with gold.

To be able to compare the SEM and SAXS/USAXS results, samples for the SEM experiments were prepared in the same rotating synthesis cell as used for the SAXS and USAXS experiments, and under the same conditions. After rapid cooling of the cell to room temperature, the sample was filtered and washed extensively with deionized water before drying and calcination.

N_2 Adsorption−Desorption Experiments. The distribution of pores was measured by the nitrogen adsorption method at liquid nitrogen temperature on a Tri-Star 2000 (Micromeritics Co.) using standard continuous procedures. Samples were degassed at 150 °C) for 5 h under reduced pressure prior to each measurement. The surface area was determined by the BET method[41] in the 0.05−0.3 relative pressure range. The Barrett−Joyner−Halenda (BJH) method was used to analyze adsorption and desorption curves. Because this technique requires much larger samples as produced by in situ synthesis in the rotating cell, silicas were prepared in the laboratory (as described in the first part of the Experimental Section) and the dried and calcined powders were investigated both by USAXS/SAXS at ESRF and BET/SEM.

Results

Combined USAXS/SAXS. Silica was prepared in situ in the dedicated USAXS/SAXS rotating cell and X-ray scattering spectra were recorded continuously. The obtained merged USAXS/SAXS results are presented in Figure 2. Because of the variations in thickness of the silica (due to the precipitation of the aggregated silicas in the very narrow rotating cell) the USAXS pattern sometimes is noisy with the consequence that the periodicity of the rotating cell (0.5 cycle/minute) can be recognized easily during the 10 min scan (for an example see the lower and middle curves in Figure 2e). When the fractal systems have only a relatively short fractal range, the SAXS profiles will appear as several short straight lines. The explanation of such fractals contains uncertainties. Therefore it is necessary to combine other characterization results, e.g., BET and SEM data for an accurate structure interpretation. Further, in the upper Q region the SAXS data sometimes are out of the limit of detector, so the electron intensity is quite low. After data treatment, e.g., normalization and background subtraction, the curve appears flat (for an example see the lower and middle curves in Figure 2c,d). As expected, the SAXS spectra were very smooth because of the application of a position sensitive

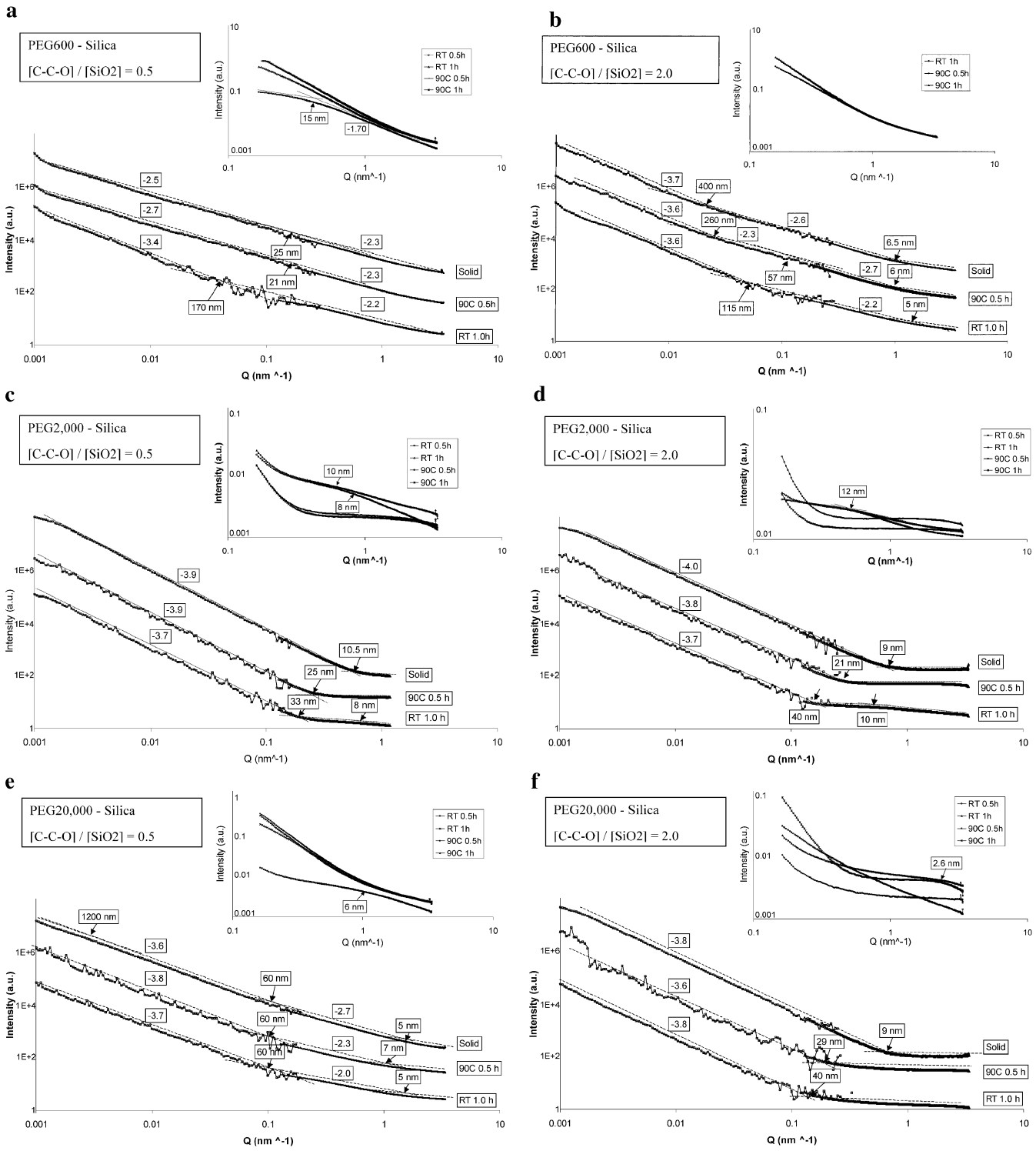

Figure 2. Merged USAXS−SAXS patterns of in situ reaction mixtures after 1 h at RT (lower curve), of 1 h RT plus 0.5 h at 90°C (middle curve), and of powdered silica after calcination (upper curve). Inset: SAXS patterns of in situ reaction mixtures with expanded intensity scale (no vertical shifts). a: PEG600/silica = 0.5. b: PEG600/silica = 2.0. c: PEG2,000/silica = 0.5. d: PEG2,000/silica = 2.0. e: PEG20000/silica = 0.5. f: PEG20,000/silica = 2.0.

detector instead of scanning. However, as a precaution, many (10−20) snapshots of 1 s were taken, but in general the reproducibility was excellent (apart from absolute intensity) and therefore only one curve is shown for each sample (Figure 2a−f). The smooth spectra were also obtained for powdered solid samples, treated by calcination (upper curves in Figure 2a−f).

For PEG600-silica aggregation at the low molar ratio, in the log(I)−log(Q) plot (Figure 2a) slopes of −3.4 and −2.2 were observed after 1 h at RT in the low Q (USAXS) and high Q (SAXS) region, respectively. Most probably, the gel is composed of micron-sized homogeneous flocs with a very irregular (fractal) surface, with a fractal surface dimension (D_s) of 6−3.4 = 2.6. The building blocks of these flocs are (reaction limited[2,42]) fractal aggregates with fractal dimension D = 2.2 and a size of approximately 170 nm. After the temperature was increased to 90 °C, the low Q slope is increased to −2.5. Aging must have transformed the flocs into a fractal system, albeit with a fractal dimension clearly different from the observed 20−

25-nm-sized aggregates with $D = 2.3$. This pattern is preserved after drying and calcination (upper spectrum of Figure 2a).

The silica aggregation mediated by PEG600 at the high ratio of 2.0 (Figure 2b) is more complicated. Similar to the low ratio preparation, at RT slopes of -3.6 (low Q) and -2.2 (high Q) are observed, again suggesting the presence of large homogeneous flocs with an irregular surface and again are build from fractal, but now smaller (115 nm), aggregates. Only above $Q = 1$ nm^{-1} the presence of 5 nm-sized primary particles is observed (bottom curve in Figure 2b). However, at higher temperatures the large flocs are now preserved, although the fractal aggregates continue to grow to 260 nm (1 h at 90 °C) and 400 nm (after calcination). At the same time the fractal dimension of the aggregates also increases considerably (from 2.2 to 2.7 and 2.6), probably because the aging process has changed the fractal structure: the "2.2-structure" is slowly replaced by the other structure, together with a growth (5 → 6 → 6.5 nm) of the primary particles.

With PEG2000 instead of PEG600 the reaction proceeds quite differently, because now the fractal aggregates are absent (see Figure 2c,d). Here, the homogeneously distributed big flocs (with only surface fractality as indicated by the slopes close to -4,[2,42] and further smoothened during aging at 90 °C) are built directly from homogeneous 8−12-nm-sized particles; see insets with SAXS spectra in Figure 2c,d. As also demonstrated by the curves in these insets, during aging at 90 °C, these particles become converted into much smaller particles, characterized by a broad band at the 2−3 nm^{-1} region. Remarkable is the loss in scattering intensity during this conversion, as shown by the right-shift of the transition from the USAXS to the SAXS region (at 33 → 10.5 and 40 → 9 nm, respectively, for low and high PEG2000/silica ratios).

Experiments with PEG20000 at PEG/silica = 2.0 strongly resemble the PEG2,000 results but only at the high ratio (Figure 2f). Again fractal aggregates are absent, but the intensity shift in the SAXS region is less pronounced and the surface of the large flocs is slightly rougher ($D_s = 3.7$). Only a very broad featureless intensity appeared after 0.5 h during the reaction at RT, but this was soon transformed into a curve very similar to that of the low PEG2000/silica synthesis (Figure 2c). With the low PEG/silica ratio (Figure 2e), fractal aggregates show up again, similar to the PEG600 systems. Only during the first part of the reaction at RT nonfractal 6-nm-sized particles are present, similar to the PEG2000 system.

SEM. After the synthesis, the six PEG-mediated silicas were dried and calcined; SEM images showing the particle texture of these samples are displayed in Figure 3a−f.

Silica mediated by PEG600 at low molar ratio exhibits large particles of approximately 1−10 μm. Most probably they coincide with the large flocs as revealed by USAXS in the reaction mixture (Figure 2a, low Q region), with the fractal character of the flocs preserved after drying and calcination and resulting in the very rough surface of the particles (Figure 3a). The building blocks of these aggregates probably are the 25 nm fractal particles (inset in Figure 3a); these particles can be discerned at the resolution limit of the SEM. However, particles or pores below 20 nm cannot readily be observed, because of the gold coating obtained by sputtering of the sample prior to examination.

As may be expected from the USAXS region in Figure 2b, the sample with high molar ratio of PEG600/SiO_2 shows very different SEM images (Figure 3b) in comparison to the low molar ratio: both the SEM and USAXS data now show rather smooth (but very irregular) particles. The fractality of the surface as indicated by USAXS is visible as a quite rough surface in the SEM image. These irregular particles are composed of approximately 500 nm primary particles and may be correlated with the 400 nm aggregates of Figure 2b.

PEG2,000 provides well-defined spherical and very smooth (nonfractal) silica particles with sizes between 1 and 6 μm (Figure 3c,d), which is again in agreement with the USAXS results. The SAXS spectra (inset in Figure 2c,d) show that (almost) no particles of 8−10 nm are present after heating, and this corresponds with the observation of very smooth particles in Figure 3c,d.

Both the USAXS data and SEM image of PEG20000 (high ratio) correspond with the data of PEG2000 (for both ratios) as shown by figures 2f and 3f. Only structures at low ratio synthesis with PEG20000 are clearly different, because of the presence of (fractal) aggregates on the surface of spherical particles (Figure 3c). Nevertheless, a very good agreement with the USAXS results (Figure 2e) is obtained: a rough surface (slope $= -3.6$) of the particles, and the 60-nm-sized fractal aggregates may be assigned as the partial coverage of the big particles as shown at the SEM image of Figure 3e.

N_2 Adsorption−Desorption Experiments. Nitrogen adsorption isotherms are displayed in Figure 4a−f. The isotherm of the low ratio PEG600-silica (Figure 4a) can be classified as type IV,[41] with a steep increase in nitrogen uptake and a big adsorbed hysteresis loop at high relative pressure p/p_0 0.8−1.0, typical for a mesoporous solid with rather big pores (according to the IUPAC classification mesopores are between 2 and 50 nm[41]). Although the high ratio PEG600-silica (Figure 4b) looks different, it may also be classified as type IV, but now with a wide hysteresis loop at p/p_0 0.45−0.9. Again we are dealing with a mesoporous solid, but now with smaller pores. This is confirmed by applying the Barret−Joyner−Halenda (BJH) method to calculate the pore size distribution. These results indicate that the low ratio sample (inset Figure 4a) has pores peaking at 20 nm in diameter with relatively broad pore size distributions, while the high ratio sample (inset Figure 4b) is characterized by pores averaging 4 nm in diameter (Table 1).

On the other hand, the N_2 adsorption−desorption isotherms (main plot) for PEG2000 silicas are type I,[41] typical for microporous solids (pore diameter below 2 nm; Figure 4c,d). Accordingly, the pore size distribution shows only pores below 4 nm in diameter (insets of Figure 4c,d). Although with SEM it is very difficult to distinguish pores below 20 nm in the big silica particles, the smoothness of the spheres in Figure 3c,d compared to the roughness in Figure 3a,b is in accordance with the suggested presence of micropores and mesopores, for the PEG2000 and PEG600 silicas, respectively.

Also observations on PEG20000 at a high ratio of PEG/SiO_2 fits in this scheme (Figure 4f); again smooth spheres, as also determined by SEM (Figure 3f), correspond with an isotherm representing a microporous solid with submicron pores.[41] As could be expected, for PEG20000 at a low PEG/SiO_2 ratio again is different (Figure 4e): the rough coverage of the spheres (Figure 3e) implies the presence of both micropores and mesopores, and the isotherms fit this expectation, although both the width of the hysteresis loop and the relative quantity of the 3 nm pores suggest less mesoporosity compared to the PEG600 systems.

The presence of mesopores in PEG600 silicas is also characterized by the increase in pore volume, corresponding with a decrease in surface area (Table 1); moreover, the increase in adsorbed nitrogen gas at high p/p_0 is caused by multilayer

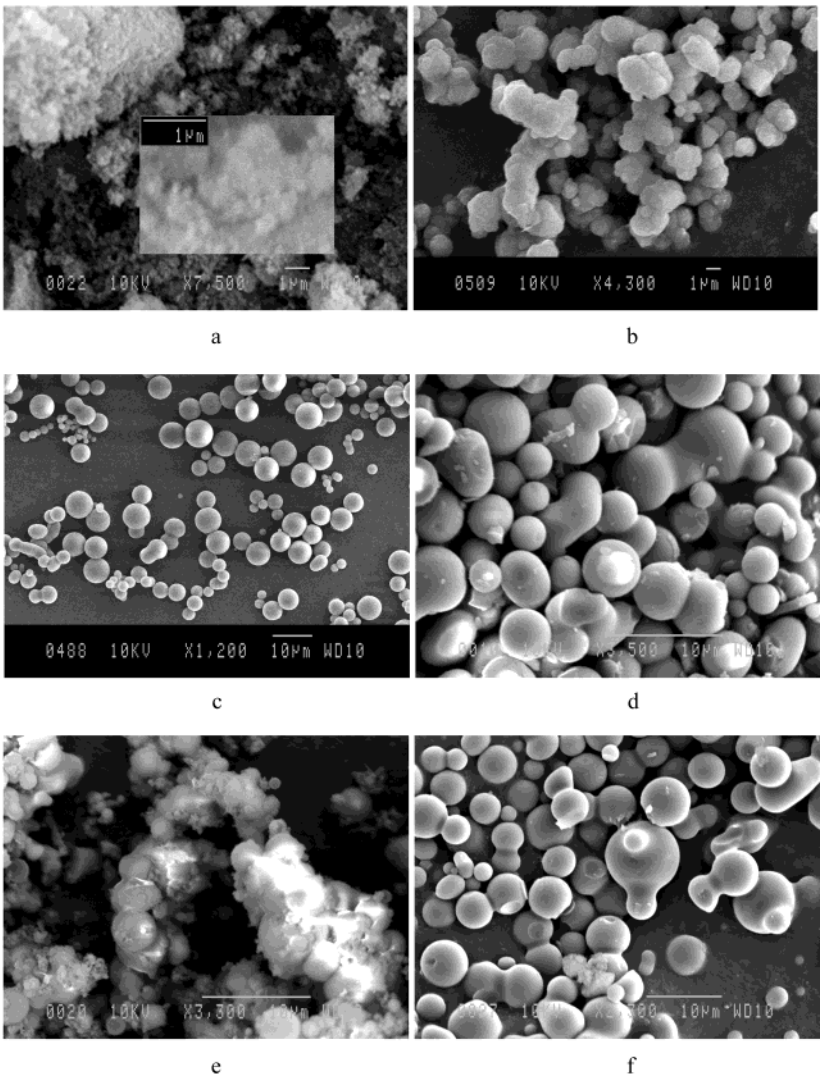

Figure 3. Scanning electron microscopy (SEM) images of dried and calcined silicas. a: PEG600/silica = 0.5. b; PEG600/silica = 2.0. c: PEG2000/silica = 0.5. d: PEG2000/silica = 2.0. e: PEG20,000/silica = 0.5. f: PEG20,000/silica = 2.0. Scale bar measures the size in microns as indicated.

adsorption and hysteresis has to be expected. In PEG2000 silicas the picture is the opposite: micropores cause the adsorption of nitrogen in the low p/p_0 region without appreciable multiplayer adsorption or hysteresis. Only the low ratio PEG20000 silica seems to be a kind of hybrid: with two distinct maxima in the pore distribution (at 3.5 and below 2 nm) both micropores and mesopores are present in considerable quantities. Probably the micropores are related to the big silica spheres while the fractal (see Figure 2e) silica between and on the surface of these spheres is mesoporous.

Discussion

In view of the slopes in Figure 2a,b, fractal aggregates were apparently formed from primary particles. In contrast to similar experiments without PEG,[43,44] both the fractal dimension and aggregate growth are slightly higher. Striking however is the much shorter gelation time: from hours back to minutes. The growth of primary (sub)nanometer silica particles hardly changed: although PEG clearly controls the direction of growth, since the rate of the condensation reaction between ≡Si−OH and O^-−Si≡ groups is still catalyzed by OH^- and therefore fixed by pH.[1] Similar to templates in zeolites, silica can be wrapped up around one or more PEG molecules, forming spheres with diameters from approximately 1.5 nm (one PEG molecule) to 5 nm (approximately 35 PEG molecules). The slight upward bend at the very right in Figure 2a,b possibly indicates the presence of particles in this range; with particles below 1.5 nm the slope showed have been straight. Slopes around −2 are very common in log(I)−log(Q) plots during silica preparation and have to be ascribed to fractal aggregates.[2,19,42−44] However, the value of −2.2 in both Figure 2a,b is slightly lower than expected, because −2.2 is representative for aged (reorganized) systems. In general, during the first hours of the silica formation without PEG or other templates, the reactive elementary particles combine into diffusion-limited aggregates with slopes around −1.8, and only after many days (or higher reaction temperatures) the aggregates slowly transform into systems with lower density gradients. Clearly, the presence of PEG accelerates this transformation, as confirmed by the SAXS results after 0.5 h. As shown (inset in Figure 2a), the SAXS pattern corresponds with 15-nm-sized aggregates with fractal dimension of 1.70, representative for the first stage of a diffusion-limited process similar to silicas without PEG or other organics. In the next 0.5 h, the bigger PEG-silica particles are cemented together to a more compact structure using PEG as flocculation agent, resulting in the lower fractal dimension of −2.2. The reorganization of PEG-bonded silica particles is fast compared to the

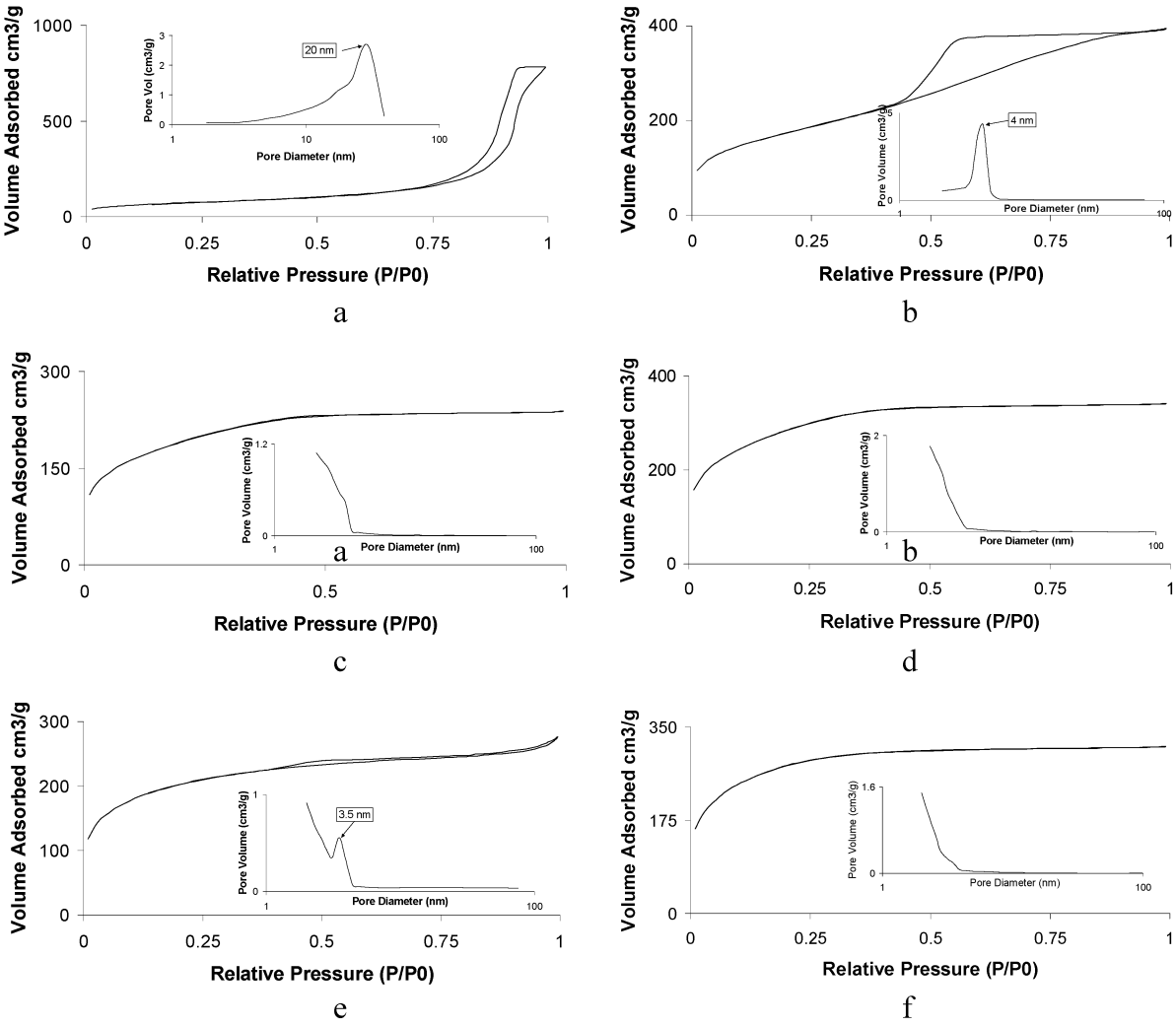

Figure 4. Nitrogen adsorption−desorption isotherms of dried and calcined silicas. Inset: Pore diameter versus pore volume according to the Barrett−Joyner−Halenda method (desorption d*V*/d*l*og(D)). a//: PEG600/silica = 0.5. b: PEG600/silica = 2.0. c: PEG2000/silica = 0.5. d: PEG2,-000/silica = 2.0. e: PEG20000/silica = 0.5. f: PEG20000/silica = 2.0.

TABLE 1: Characteristic Pore Data of the Calcined PEG-Silica

sample	PEG/silica ratio	surface area (m^2/g)	specific pore olume (cm^3/g)	average pore diameter (nm)
PEG600	0.5	258	1.21	20
PEG600	2.0	636	0.65	4.0
PEG2000	0.5	687	0.23	<2
PEG2000	2.0	1030	0.32	<2
PEG20000	0.5	720	0.25	<2 and 3.5
PEG20000	2.0	993	0.22	<2

aging of silica without templates, because in the latter covalent Si−O−Si bonds have to be hydrolyzed.

At much larger scale the aggregates first combine in almost structure-less flocs (slopes are −3.4 and −3.6, respectively). As mentioned earlier, this is a very fast process and gels are formed within minutes. This is a striking difference with the silicas without PEG, where the combination of silica aggregates into gels may require one hr or more at this concentration. The flocs recombine (in the system with the low PEG/silica ratio) in a superaggregate with only slightly higher fractal dimensions. Most of the space between the aggregates will no doubt be filled with PEG (inducing phase separation and/or capillary effects) and only at the border of the flocs empty spaces between the aggregates will be responsible for a rough surface with the fractal surface dimensions of 2.6 to 2.3 (Figure 2a,b, low *Q* region). During aging at 90 °C the ratio of silica and PEG is very important. With a surplus of PEG no structural change is observed and the floc structure is preserved during heating, drying and calcination. With a surplus of silica, however, there is not enough PEG to maintain all the bonds between the aggregates, and a branched structure should be expected to appear,[46] concentrating most of the inter-aggregate bonds in the center of the big floc and resulting in fractal dimensions of 2.7 and 2.5 after heating and drying/calcination, respectively. This same phenomenon has been observed during drying of silica solutions.[46] This contrast at large scale between high and low PEG/silica ratio can also be observed in the aforementioned SEM and BET results: at low ratio the fractals are preserved (Figure 3a), at high ratio the micrometer-sized particles appear to be very homogeneous (Figure 3b), in accordance with the surface fractal dimension D_s of 2.3 ($D_s = 6 - (-\text{slope})$).[42] During drying and calcination the rough surface has been smoothened, probably driven by the principle of minimizing surface tension.[1] The BET plots of figures 4a and 4b confirm this situation: large mesopores are due to the protection of the interstices between the aging-enforced branches of the fractals, and only 3.5 nm pores are present in the more compact clustering of 6.5 nm particles, resulting in the smaller and so-called ink-bottle-shaped pores[41] that can be deduced from the hysteresis loop in Figure 4b.

As expected,[19,37] silica preparations with PEG2,000 produced very different results because the flocculation abilities of the much longer PEG polymers prevent the free diffusion of particles or clusters, a necessary condition to form fractal structures; only PEG-cladded and PEG-connected silica particles are formed. These very big, homogeneous and stable flocs precipitate, collapsing to dense structures during drying and calcination, because of the burning of the connecting PEG polymers. By minimizing the surface energy of the particles[1] a smooth surface is formed. However, the change at nanometer scale is more difficult to explain. Contrary to the PEG600 syntheses, now the 8 nm particles disappear after heating the reaction mixture (see inset in Figure 2c,d), to be replaced by 3 nm particles. Again the removal of PEG could be the cause: the 8 nm particles probably are small clusters or flocs, composed of silica particles covered by a PEG polymer that are only connected with one particle. This can also be the reason that at high PEG/silica ratio these clusters are bigger: 12 nm compared to 8 nm.

Because in USAXS the contribution of the big particles is much more important, in Figure 2c,d only a very slight downward bending can be observed at 0.001 nm^{-1} ($\approx 6\ \mu m$). In Figure 4c,d it is shown that the calcined samples only have micropores ($d < 2$ nm), probably the cavities between the solid 3 nm particles.

Applying PEG20000, the most striking feature is that the properties of these silicas do not suit the 600−2000 trend from fractal silicas to smooth spheres. Here, on the surface of the silica spheres again fractal silica can be observed, especially at the low PEG/silica ratio. But these aggregates are not similar to the PEG600 aggregates: especially the big change in fractal dimension at room temperature ($D_m = 2.0$) and after calcination ($D_m = 2.7$), in comparison to $D_m = 2.2$ and $D_m = 2.3$ for PEG600 silicas) suggest a different aggregation mechanism. This is confirmed by BET where again micropores are observed in addition to mesopores with a much smaller diameter ($d = 3.5$ nm compared to 20 nm for the low ratio PEG600 system; Figure 4e) and the presence of bigger mesopores with a very wide pore distribution ($d_{ave} \approx 20$ nm; inset of Figure 4e). These large pores correspond with the upward part of the very long hysteresis loop of the adsorption isotherm and according to the SEM image (Figure 3e) the biggest pores are present at the rough surface. The smaller 3.5 nm pores are the crevices in the more homogeneous ($D = 2.7$: relatively small density gradient) silica, occupied by the long PEG20,000 polymers during the preparation. The high ratio PEG20000/silica is much more similar to the PEG2000 system: no fractal aggregates and only very small heterogeneities on the almost smooth surface of the big spheres.

To explain the influence of PEG on the polymerizing silica, first it is important to realize that probably the growing aggregates, spheres, or other polymorphs of silica not only are steered by PEG but also that the reverse is possible: the conformation of this polymer can be directed by silica. The interaction between a flexible membrane and a dissolved polymer has been analyzed by Kim and Sung,[45] who showed that the membrane can bend by an adsorbing polymer both in a concave and convex way, depending on the ratio between entropy and binding interactions. Because also silica polymers are very flexible (the activation energy of bending the Si−O−Si angle is very low[1]), silica may be able to form a shell around PEG (similar to templates in zeolites) or the other way round: silica will be enclosed by PEG. Because of the entropy term the first situation would be especially important for relatively small PEG molecules, for example, PEG600.

Flocculation (connection of silica spheres by polymers interacting with two or more spheres) might be important in the very beginning of the preparation, but probably not in the way as described by Iler.[1] Instead of big silica spheres connected by polymers, the very fast gelation might be caused by connection of PEG polymers by (very small) silica spheres. In this case, the gel network is composed mainly of PEG instead of silica, and the majority of the silicic acid monomers and oligomers are still in solution. When the preparation proceeds, silica spheres grown at suitable sites all over the PEG (and may enclose small PEG molecules, if present) and will be connected by a very dense interparticle network of PEG.

This flocculation might be the most important distinction between silica prepared by small and large PEG. Especially the very large PEG20,000 will be entangled in a mass of silica spheres, and enclosure by silica or phase separation will be almost impossible. This network might be very dense at high PEG20,000/silica ratios, preventing the diffusion of silica particles to form fractal aggregates. In contrast, the small PEG600 might be encapsulated by silica or form pools within the silica framework. This observation is in accordance with presented data by Iqbal and Ballesteros,[47] who found that small molecules become completely encapsulated; this encapsulation depends on a certain threshold defined by the size of the molecule, its entropy, and its hydrophobicity. The big mesopores in the PEG600 silica may originate from this latter effect. Finally, PEG2000 may only be present at the surface of the silica spheres, forming connections between spheres at a small scale (compared to the 10 times larger PEG20000). Reorganizations at higher temperatures will result in better dissolution of PEG in the water phase and therefore in dense silica spheres with only micropores. Concerning the differences between the low and high PEG/silica ratio experiments, the dissolution of PEG in the water phase and the corresponding phase separation by silica-PEG interactions is obviously important, especially for the PEG20000 silicas, resulting in relatively large differences between high and low ratio of PEG/silicas. Moreover, if water glass is replaced by TEOS, the alcohol formed by the hydrolysis of TEOS will make comparisons between these experiments very tricky. In recent additional experiments with addition of organics, silicas with totally different morphologies at both micro- and nanometer scale were obtained.[48]

Investigation of the synthesized PEG-silicas by nitrogen adsorption also shows that several types of pores are present: interparticle (textural) and framework-confined (structural) porosity can be discerned, based on evidence from the adsorption step and the uptake of nitrogen gas above a partial pressure of 0.80.[49] In general, the mesopores revealed by the pore size distribution curve correspond to interstices among fractals. These textural pores are very large, in agreement with the N_2 adsorption isotherm that shows a hysteresis loop at high partial pressure, and with the pore size distribution curve. Much smaller are the structural pores: these are the micropores, probably corresponding with the interstices between the small elementary particles, from which the smooth silica spheres in the PEG2,-000 silicas are composed.

A general overview of the PEG-silicas is presented in Figure 5. As a general rule it can be stated that increase in hydrophobicity (both because of the increase in PEG/silica ratio and in size of the PEG polymer) results in a larger surface area and a more uniform pore size distribution. However, due to the complications induced by different combinations of flocculation properties (interparticle bonding) and template or structure-directing properties, no clear linear effects can be discerned

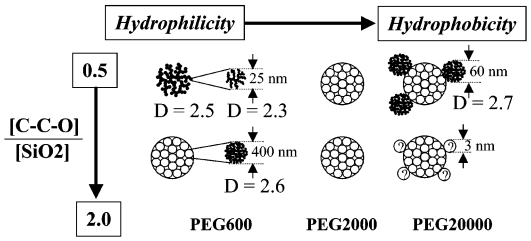

Figure 5. General overview of PEG-silicas as a function of PEG/silica ratio and size of PEG polymers. At low PEG/silica ratio (upper row), with increasing length of the PEG polymers (increasing hydrophobicity), fractal silicas (composed of fractal particles) are replaced by smooth silica spheres, covered by fractal particles using PEG20000. At high PEG/silica ratio (lower row), only at low hydrophobicity the homogeneous porous silicas are composed of fractal particles, and are covered (at high hydrophobicity) with particles. The constitution of these particles (homogeneous or fractal) is not known.

when the quantity and size of PEG is varied during PEG-silica preparations.

Conclusions

A combined USAXS/SAXS approach has been employed to investigate in situ silica aggregation in the presence of PEG polymers. In contrast to similar experiments without PEG, the aggregate growth of PEG-mediated silicas was much faster. For PEG600, the aggregates quickly combined in almost structureless flocs, then recombined in a superaggregate with only slightly higher fractal dimensions. With a surplus of PEG, no structural change was observed and the floc structure was preserved during heating, drying, and calcination. With a surplus of silica, however, a branched structure appeared, resulting in very large mesopores. In contrast, silica mediated by PEG2000 and PEG20000 produced different structures because the flocculation abilities of the much longer PEG polymers seem to prevent the free diffusion of particles or clusters. This is a necessary condition to form fractal structures; only PEG-connected silica particles were formed and very small heterogeneities on the almost smooth surface of the big spherical particles.

Apparently poly(ethylene glycol) is a versatile templating agent to prepare porous silica because of three different properties: (1) PEG is a flocculation agent in a silica sol, (2) the hydrophobic silica-PEG interactions steer the silica polymerization, and (3) phase separation, where a phase rich in both PEG and silica is formed in the formerly homogeneous water solution. The flocculation may well be the most important distinction between silica prepared with small and large PEG. In this view small PEG600 is encapsulated by silica and forms pools within the silica framework, whereas large PEG20000 is entangled in a mass of silica spheres, making enclosure by silica or phase separation almost impossible. Because the relative influence of these three effects depends both on the silica-PEG ratio and on the size of the PEG polymer coils, variations in these parameters can in principle be used to prepare tailor-made porous silicas: with PEG600 mesoporous silicas with pore sizes of 20 and 4 nm can be prepared, depending on the silica/PEG ratio, and with PEG2,000 only smooth microporous silica spheres, with diameters between 2 and 10 micron. Because of increased flocculation effects, these smooth spheres will be covered by nanometer-sized silica clusters when PEG20,000 is applied. As a general rule it can be stated that increase in hydrophobicity (both because of the increase in PEG/silica ratio and in size of the PEG polymer) results in a larger surface area and a more uniform pore size distribution.

Although we did not succeed in preparing porous silicas similar to any one of those in diatom species, we nevertheless made an important step toward this goal: we showed that even simple structure-directing agents such as PEG-polymers of different molecule lengths and different PEG/silica ratios, it is possible to create by choice silicas with pores with diameters of less than 2 nm up to 20 nm; therefore, polymers of this kind may well be a cheap and versatile substitute for biomolecules (such as proteins, enzymes or carbohydrates) involved in silica biomineralization,[8] if silicas resembling natural ones, notably the ones present in such huge diversity in diatoms, are the focus of scientific attention, e.g., for biomimicking with a view toward industrial applications.

Acknowledgment. Beam time at ESRF for combined USAXS/SAXS at beamline ID02 was granted by European Committee, whereas for the SAXS studies at the DUBBLE station (beamline BM26) a grant from Netherlands Organization for the Advancement of Pure Research (NWO) was obtained. We thank Dr. T. Narayan (ESRF), Dr. W. Bras (NWO) for assistance with experiments at the beamlines ID02 and BM26 during the measurements at ESRF, and Dr. P. C. M. M. Magusin (TUE) for helpful discussion. Q.S., S.H., and E.G.V. were supported by The Netherlands Technology Foundation (STW; Grant GFc4983), which is subsidized by NWO.

References and Notes

(1) Iler, R. K. *The Chemistry of Silica;* John Wiley & Sons: New York, 1979.
(2) Brinker C. J.; Scherer G. W. *Sol−Gel Science;* Academic Press: San Diego, 1990.
(3) Biz, S.; Occelli, M. *Catal. Rev.−Sci. Eng.* **1998**, *40*, 329−407.
(4) Round, F. E.; Crawford, R. M.; Mann, D. G. *The Diatoms;* Cambridge University Press: Cambridge, 1990.
(5) Kresge, C. T.; Leonowicz, M. E.; Roth, W. J., Varuli, J. C.; Beck, J. S. *Nature* **1992,** *359*, 710.
(6) Vartuli, J. C.; Schmitt, K. D.; Kresge, C. T. *Chem. Mater.* **1994**, *6*, 2317.
(7) Stucky G. D.; Monnier, A.; Schuth, F.; Huo, Q.; Margolese, D.; Kumar, D.; Krishnamurty, M.; Petroff, P.; Firouzi, A.; Janicke, M.; Chmelka, B. F. *Mol. Cryst. Liq. Cryst.* **1994,** *240*, 187.
(8) Vrieling, E. G.; Beelen, T. P. M.; van Santen, R. A.; Gieskes, W. W. C. *Angew. Chem., Int. Ed.* **2002**, 41, 1543−1546.
(9) Sayari, A.; Hamoudi, S. *Chem. Mater.* **2001,** *13*, 3151−3168.
(10) Vrieling, E. G.; Beelen, T. P. M.; van Santen, R. A.; Gieskes, W. W. C. *J. Biotechnol.* **1999,** *70*, 39−51.
(11) Vrieling, E. G.; Gieskes, W. W. C.; Beelen, T. P. M.; van Santen, R. A. *J. Phycol.* **2000,** *36*, 146−159.
(12) Shimizu, K.; Cha, J.; Stucky, G. D.; Morse, D. E. *Proc. Natl. Acad. Sci. U.S.A.* **1998,** *95*, 6234−6238.
(13) Morse, D. E. *TIBTECH* **1999,** *17*, 230−232.
(14) Cha, J. N.; Stucky, G. D.; Morse, D. E.; Deming, T. J. *Nature* **2000,** *403*, *289*−*292*.
(15) Kröger, N.; Deutzmann, R.; Sumper, M. *Science* **1999,** *286*, 1129−1132.
(16) Mann, S. *Angew. Chem., Int. Ed.* **2000,** *39*, 3392−3406.
(17) Faraone, A.; Magazu, S.; Maisano, G.; Migliardo, P.; Tettamanti, E.; Villari, V. *J. Chem. Phys.* **1999,** *110*, 1801−1806.
(18) Armstrong, J. K.; Leharne, S. A.; Stuart, B. H.; Snowden, M. J.; Chowdhry, Z. *Langmuir* **2001,** *17*, 4482−4485.
(19) Ågren, P.; Counter, J.; Laggner, P. *J. Non-Cryst. Sol.* **2000,** *261*, 195−203.
(20) Blin, J. L.; Becue, A.; Pauwels, B.; van Tendeloo, G.; Su, B. L. *Microporous Mesoporous Mater.* **2001,** *44*−*45*, 41−51.
(21) Dahmouche, K.; Santilli, C. V.; Pulcinelli, S. H. *J. Phys. Chem. B* **1999,** *103*, 4937−4942.
(22) Göltner, C. G.; Smarsly, B.; Berton, B.; Antonietti, M. *Chem. Mater.* **2001,** *13*, 1617−1624.
(23) Hubert, D. H. W.; Jung, M.; Frederik, P. M.; Bomans, P. H. H.; Meuldijk, J. German, A. L. *Adv. Mater.* **2000,** *12*, 1286−1290 and 1291−1294.
(24) Kim, S. S.; Karkamkar, A.; Pinnavaia, T. J.; Kruk, M.; Jaroniec, M. *J. Phys. Chem. B* **2001,** *105*, 7663−7670.
(25) Krakovsky, I.; Urakawa, H.; Kajiwara, K.; Kohjiya, S. *J. Non-Cryst. Sol.* **1998,** *231*, 31−40.

(26) Lesot, P.; Chapuis, S.; Bayle, J. P.; Rault, J.; Lafontaine, E.; Campero, A.; Judeinstein, P. *J. Mater. Chem.* **1998,** *8*, 147−151.
(27) Prouzet, E.; Pinnavaia, T. J. *Angew. Chem., Int. Ed.* **1997,** *109*, 5533−536.
(28) Sierra, L.; Guth, J.-L. *Microporous Mesoporous Mater.* **1999,** *27*, 243−253.
(29) Smarsly, B.; Polarz, S.; Antonietti, M. *J. Phys. Chem. B* **2001,** *105*, 10473−10483.
(30) Takahashi, R.; Nakanishi, K.; Soga, N. *J. Sol-Gel Sci. Technol.* **2000,** *17*, 7−18.
(31) Wang, L.; Wang, Z.; Zhao, J.; Yuan, Z.; Yang, H.; Zhao, M. *Mater. Chem. Phys.* **1999,** *59*, 171−174.
(32) Zhao, D.; Huo, Q.; Feng, J.; Chmelka, B. F.; Stucky, G. D. *J. Am. Chem. Soc.* **1998,** *120*, 6024−6036.
(33) Cheng, Y.-R.; Lin, H.-P.; Mou, C.-Y. *Phys. Chem. Chem. Phys.* **1999,** *1*, 5051−5058.
(34) Rutland, M. W.; Senden, T. J. *Langmuir* **1993**, *9*, 412−418.
(35) Gulley, G. L.; Martin, J. E. *J. Coll. Interface Sci.* **2001,** *241*, 340−345.
(36) Wong, K.; Lixon, P.; Lafuma, F.; Lindner, P.; Charriol, O. A.; Cabane, B. *J. Coll. Interface Sci.* **1992,** *153*, 55−72.
(37) Vonk, C. G. *J. Appl. Crystallogr.* **1973,** *6*, 81.
(38) Diat, O.; Bösecke, P.; Lambard, J.; de Moor P.-P. E. A. *J. Appl. Crystallogr.* **1997,** *30*, 862−866.
(39) De Moor, P.-P. E. A.; Beelen, T. P. M.; van Santen, R. A.; Beck, L. W.; Davis, M. E. *J. Phys. Chem. B* **2000**, *104*, 7600−7611.
(40) De Moor, P.-P. E. A.; Beelen, T. P. M.; Komanschek, B. U.; Beck, L. W.; Wagner, P.; Davis, M. E.; van Santen, R. A. *Chem. Eur. J.* **1999,** *5*, 2083−2088.
(41) S. J. Greg and K. S. W. Sing, *Adsorption, Surface Area and Porosity*, 2nd ed.; Academic Press: London, 1995.
(42) Martin, J. E.; Hurd, A. J. *J. Appl. Crystallogr.* **1987,** *20*, 61−78.
(43) Wijnen, P. W. J. G.; Beelen, T. P. M.; Rummens, C. P. J.; van Santen, R. A. *J. Non-Cryst. Sol.* **1991,** *136*, 119−125.
(44) Beelen, T. P. M.; Dokter, W. H.; van Garderen, H. F.; van Santen, R. A. *Adv. Coll. Interface Sci.* **1994,** *50*, 23−37.
(45) Kim, Y. W.; Sung, W. *Phys. Rev. E* **2001,** *63*, 041910−1−041910−5.
(46) Beelen, T. P. M.; Shi, W. D.; Morrison, G. R.; van Garderen, H. F.; Browne, M. T.; van Santen, R. A.; Pantos, E. *J. Colloid Interface Sci.* **1997,** *185*, 217−227.
(47) Iqbal, G.; Ballesteros, A. *TIBTECH* **2000,** *18*, 282−301.
(48) Sun, Q.; Hazelaar, S.; Kooyman, P. J.; Vrieling, E. G.; Gieskes, W. W. C.; Beelen, T. P. M.; Sommerdijk, N. A. J. M.; van Santen, R. A., to be submitted.
(49) Prouzet, E.; Cot, F.; Nabias, G.; Larbot, A.; Kooyman, P.; Pinnavaia, T. J. *Chem. Mater.* **1999**, *11*, 1498−1503.